AIAA JOURNAL
Vol. 41, No. 2, February 2003

Flow-Tagging Velocimetry for Hypersonic Flows Using Fluorescence of Nitric Oxide

Paul M. Danehy*
NASA Langley Research Center, Hampton, Virginia 23681
and
Sean O'Byrne,† A. Frank P. Houwing,‡ Jodie S. Fox,§ and Daniel R. Smith¶
Australian National University, Canberra, Australian Capital Territory 0200, Australia

We demonstrate a new variation of molecular-tagging velocimetry for hypersonic flows based on laser-induced fluorescence. A thin line of nitric-oxide molecules is excited with a laser beam and then, after a time delay, a fluorescence image of the displaced line is acquired. One component of velocity is determined from the time of flight. This method is applied to measure the velocity profile in a Mach 8.5 laminar, hypersonic boundary layer in the Australian National University's T2 free-piston shock tunnel. The single-shot velocity measurement uncertainty in the freestream was found to be 3.5%, based on 90% confidence. The method is also demonstrated in the separated flow region forward of a blunt fin attached to a flat plate in a Mach 7.4 flow produced by the Australian National University's T3 free-piston shock tunnel. The measurement uncertainty in the blunt fin experiment is approximately 30%, owing mainly to low fluorescence intensities, which could be improved significantly in future experiments. This velocimetry method is applicable to very high-speed flows that have low collisional quenching of the fluorescing species. It is particularly convenient in facilities where planar laser-induced fluorescence is already being performed.

Introduction

VELOCITY is one of the most important flowfield parameters to measure in nonreacting flows. The velocity field is particularly important in hypersonic flows because it describes the spatial distribution of kinetic energy, which accounts for a significant fraction of the total energy. Although several very good methods for measuring velocity in hypersonic flows exist, this paper describes a new flow-tagging method that should be particularly convenient to use in some flow facilities.

We use this new method to measure the velocity profile of the laminar boundary layer that develops on a flat plate placed in a hypersonic freestream. This flow has been studied extensively both computationally and experimentally. Good agreement has been found between predicted and measured pressure and heat-transfer distributions.[1,2] However, because of the difficulty in accurately measuring flowfield parameters in hypersonic facilities satisfactory agreement between predicted and measured density,[1,2] temperature,[3] and velocity[1] profiles within the boundary layer have not yet been realized to our knowledge.

The goal of the present experiment was to develop a method suitable for measuring the velocity in this flowfield; this velocity profile could then be compared with theoretical models that predict the flow, in an effort to validate the models. This experiment is part of a larger study of laminar hypersonic boundary layers, including heat-transfer measurements, planar laser-induced fluorescence (PLIF) temperature measurements, and computational fluid dynamics (CFD) simulations presented elsewhere.[4] To demonstrate the usefulness of this new velocimetry method to other flow configurations, we also use the technique to probe the separated flow forward of a blunt fin attached to a flat plate in a Mach 7.4 flow. This configuration simulates the wing/body, tailfin/body and strut/wing junctions on aerospace vehicles. We believe that these are the first velocity measurements of the separated flow forward of a blunt fin attached to a flat plate in supersonic or hypersonic flow.

Velocity has been measured in high-speed gas flows using a variety of different methods. Hypersonic flowfields are a challenging environment for many velocimetry techniques for several reasons. Physical probes such as hot-wire anemometers are inappropriate for studying supersonic or hypersonic flows because they disturb the flow and because their size limits the spatial precision of the measurements. In shock tunnels line or two-dimensional imaging methods are preferred to single-point methods such as laser Doppler velocimetry or laser-induced thermal acoustics[5] because the limited test time of the flow makes it very expensive to map the velocity field.

Several laser-based methods have been developed for mapping the velocity in gaseous flows. These include particle image velocimetry and planar Doppler velocimetry.[6,7] Both of these methods rely on scattering of light from particles present or seeded in the flow. In hypersonic flows particles do not always follow the flow. Also, in impulse facilities like shock tunnels it is difficult to seed particles uniformly into the flow. For this reason, methods involving scattering from molecules present in the flow are more desirable. Rayleigh-scattering velocimetry[8–10] and PLIF velocimetry are two widely used molecular-based methods. Both of these methods use the Doppler shift of the scattered light to determine the flow velocity. We found that Rayleigh-scattering velocimetry could not be used in the Australian National University's (ANU) free-piston shock tunnels because Mie scattering (from particles) overwhelmed Rayleigh scattering (from molecules) by more than an order of magnitude. A molecular absorption filter is commonly used to separate Mie and Rayleigh signals. However, we could not use an absorption filter because in the present experiment both particles and molecules were moving at hypersonic velocities in some parts of the flow and subsonic velocities elsewhere. Without a way to separate the Mie and Rayleigh signals in this flow, we abandoned that approach in favor of PLIF velocimetry. PLIF signal is spectrally separate from

Received 6 August 2001; revision received 18 September 2002; accepted for publication 2 October 2002.

*Research Scientist, Instrumentation Systems Development Branch; P.M.Danehy@larc.nasa.gov. Member AIAA.
†Ph.D. Student, Department of Physics, Faculty of Science; currently Postdoctoral Fellow, National Research Council, MS 168, NASA Langley Research Center, Hampton, VA 23681; s.b.obyrne@larc.nasa.gov. Member AIAA.
‡Reader, Department of Physics, Faculty of Science; Frank.Houwing@anu.edu.au. Member AIAA.
§Ph.D. Student, Department of Physics, Faculty of Science; js_fox@hotmail.com.
¶Honors Student, Department of Physics, Faculty of Science.

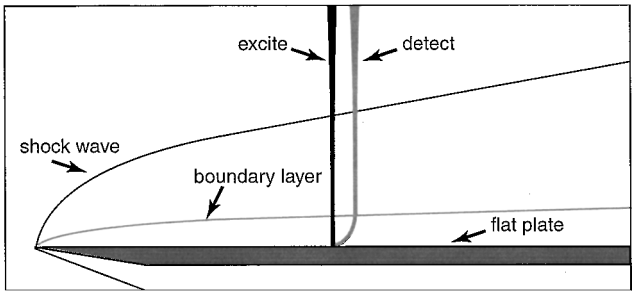

Fig. 1 Schematic of LIF flow tagging of the boundary layer on a flat plate. Flow is from left to right.

laser scatter, and therefore most elastic scattering from particles and surfaces can be filtered out. We have recently had success using PLIF to measure the radial component of velocity in ANU's T2 free-piston shock tunnel.[11] Doppler-based PLIF velocimetry has previously been used to measure two components of velocity by several authors.[12–14] However, because of the optical access limitations in ANU's shock tunnels, another method for measuring the streamwise velocity was sought.

PLIF has been used in a wide variety of velocimetry methods based on flow tagging.[15–24] In these methods time-of-flight of laser-excited molecules is used to determine the flow velocity. Unfortunately, most of these flow-tagging methods require two or even three independently tuneable and delayable pulsed lasers. One laser is typically used to write a line into the flow (via Raman excitation, dissociation, or ionization), and the second laser is used to probe the displacement of this line at a subsequent time. Hiller et al.[19] developed a flow-tagging velocimetry method requiring only a single pulsed laser. They demonstrated the technique by seeding the molecule biacetyl into a subsonic flow and observing its phosphorescence after laser excitation. Hiller et al.'s method has been used more recently by Stier and Koochesfahani[23] and also Lempert et al.,[24] who used biacetyl and acetone, respectively, to map velocity fields in subsonic flows.

Our paper extends the method of Hiller et al.[19] to a new molecule and to high-speed flows. The technique is illustrated schematically in Fig. 1. We used a tuneable pulsed laser to excite a thin line of nitric-oxide (NO) molecules that are naturally present in the shock-tunnel gas. These excited molecules fluoresce as they convect downstream. If the flow velocity is high and the test gas composition is chosen to have a low collisional quenching rate Q, then the fluorescence will continue over a short distance, for example, a few millimeters. By introducing a delay between the laser excitation pulse and the camera acquisition time, one can observe the downstream movement of the tagged molecules, from which the velocity can be simply calculated.

This method has several advantages compared to other velocimetry methods. First, it uses a single laser, which reduces cost and setup time. Second, this method is very convenient in many facilities, like the free-piston shock tunnels at the ANU, where scientists are already performing PLIF thermometry: one needs only to adjust the two sheet forming lenses (described in detail later) and delay the camera acquisition time to measure the velocity. Third, the analysis of the raw data to obtain velocity is straightforward. Fourth, compared to single-point techniques the method is advantageous because it can measure velocity along a line in the flow during a single laser pulse, and it can be extended to measure multiple velocity components over a two-dimensional region of flow by projecting a grid of laser beams, as demonstrated in Ref. 23. Finally, the method uses much lower pulse energy (~1 mJ) compared to many other flow-tagging methods (e.g., RELIEF[16] typically uses hundreds of millijoules to tag the molecules), so that the likelihood of damage to expensive aerospace vehicle models is reduced, as are systematic errors as a result of surface heating from the incident radiation. The most notable disadvantage of the method is that the flow velocity u must be on the order of, or greater than, w/τ_{LIF}, where w is the laser sheet width and τ_{LIF} is the fluorecence lifetime. This limitation restricts the application of this method to high-velocity, low collisional quenching flow environments.

Theory

Fluorescence Tagging Velocimetry Method

The PLIF method has been used extensively in fluid mechanics and to study combustion (see Refs. 25 and 26 and references therein). PLIF uses a laser to promote molecules from their ground states to excited states. Once in the excited state, the molecules fluoresce. This fluorescence is captured by a digital camera. Many PLIF measurement techniques (thermometry, Doppler-based velocimetry, mole fraction imaging, etc.) require a detailed understanding of the PLIF excitation and fluorescence process, including the accurate knowledge of the absorbing molecule's spectroscopy and energy transfer rates. However, the present method only depends on one critical parameter: the fluorescence lifetime $\tau_{\mathrm{LIF}} = 1/(A + Q)$, where A is the spontaneous emission rate and Q is the collisional quenching rate. Assuming that the laser pulse duration τ_L is much shorter than τ_{LIF}, the time evolution of the fluorescence intensity is given by

$$I_{\mathrm{LIF}} = I_{\mathrm{LIF}o} \exp(-t/\tau_{\mathrm{LIF}}) \tag{1}$$

where $I_{\mathrm{LIF}o}$ is the fluorescence intensity at the end of the laser pulse (i.e., the start of the exponential decay).

Nitric-oxide laser-induced fluorescence is a particularly appropriate optical measurement scheme for use in shock tunnels. NO is generated naturally by the shock-heating process during normal operation, which means that toxic gas handling systems are not required to seed NO into the flow. Furthermore, the NO mole fraction can be adjusted between 0 and ~8% by varying the ratio of O_2/N_2 in the shock tube gas.

For the first excited electronic state of NO that is populated by the laser in this experiment, A has been measured to be $\sim 1/(220\ \mathrm{ns})$.[27] Thus, in the absence of quenching collisions $\tau_{\mathrm{LIF}} = 220$ ns. Increasing Q always reduces the fluorescence lifetime. Paul et al.[27] provide rate constants and formulas for computing the collisional quenching rates for NO when colliding with other species. Of interest in the current work is that O_2 quenches NO fluorescence over three orders of magnitude more efficiently than N_2. For fluorescence flow-tagging velocimetry we can improve the signal-to-noiseratio of the acquired images by mimimizing Q, thereby maximizing τ_{LIF} so that the fluorescence is long lived. The longer the fluorescence lasts, the longer the delay that can be used between the laser and camera, and the more sensitive the velocity measurement.

Once the delayed fluorescence images are acquired, they must be processed to determine the displacement of the tagged gas. We have used an algorithm provided by Glenn Diskin from NASA Langley Research Center, Hampton, Virginia. The algorithm first smooths the raw data by convolving the raw image with a 3 by 4 pixel wide Gaussian function (oriented so that there is less smoothing in the streamwise direction). Next, the maximum intensity along each row of the image (in the streamwise direction) is determined. Finally, a quadratic polynomial is fit to the three pixels nearest the maximum along that row to determine the center of the displaced line. This process is repeated for each row in the image to determine displacement as a function of height above the flat plate.

If the laser sheet is not oriented perpendicular to the flow, then the method just described can lead to a systematic error in the measured velocity. To account for this laser-sheet misalignment, we obtain a fluorescence image prior to each shot in the tunnel by filling the test chamber with static gas containing a small amount of NO. This image is analyzed at the same time as the delayed flowfield images, and the static gas measurement is subtracted from the flow measurement to correct for laser-sheet misalignment.

In general, time-of-flight velocity is determined from

$$u = d/\tau_d \tag{2}$$

where u is the flow velocity, d is the displacement measured from the images, and τ_d is the delay between the laser pulse and the camera acquisition. However, this is only true in the limit that the laser pulse duration τ_L and the camera gate duration, τ_G are negligible compared to τ_d. For the boundary-layer measurements τ_d varies from 250 to 750 ns, whereas τ_L is 20 ± 3 ns and τ_G is 30 ± 3 ns.

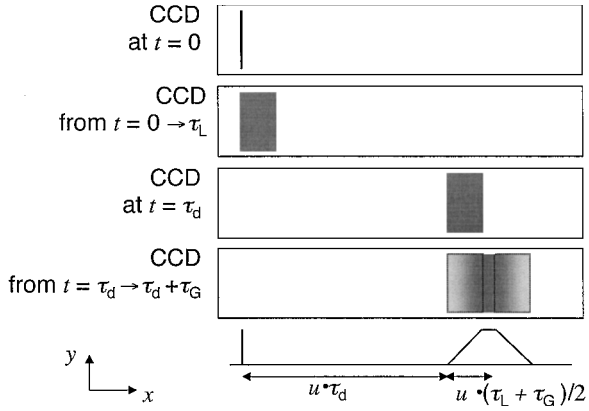

Fig. 2 Schematic of images that would be acquired by a CCD camera at different delays and gate durations during the experiment.

For the blunt fin measurements τ_d is 500 ns, τ_L is 9 ± 2 ns, and τ_G is 20 ± 3 ns. Thus, these durations are significant and need to be considered in the present work.

Figure 2 shows a schematic that explains how we derived the appropriate delay time to use in the analysis of the data. In drawing this figure, simplifying assumptions were made to isolate the most important physics of the process. In particular, we assumed that the laser sheet is infinitely thin spatially, and we neglected the fact that the intensity of the fluorescence decays exponentially during the experiment. In fact, the ~6.5 pixel width of the laser sheet does not introduce a systematic error into the measurement because the width of the sheet does not shift the center of the tagged line. The finite width does, however, reduce the sensitivity of the measurement because it broadens the tagged line, making it harder to identify the center of the line. The second assumption is not particularly good: the LIF intensity does decay slightly during the measurement time. If the tagged line were infinitely narrow spatially, the fluorescence would decrease exponentially with distance in the acquired image. The fitting algorithm just described would then produce a systematically low velocity. Because the flow moves less than 2 pixels during the image acquisition time, we calculate the systematic error from this effect to be approximately $\frac{1}{20}$th of a pixel, which is small compared to other errors in the experiment. In this figure and derivation we also assume that the laser pulse and camera gate each have square top-hat temporal profiles. Futhermore, we neglect diffusion because it acts to broaden, but not shift, the tagged line of molecules.

Figure 2 shows the fluorescence image that would be obtained at various times in the experiment. The top panel [charge-coupled device (CCD) at $t = 0$] shows how the fluorescence image would look on a CCD camera just after the laser turned on, assuming that the camera gate duration was infinitesimal (say < 1 ns). The second panel (CCD from $t = 0 \rightarrow \tau_L$) shows the image that would be obtained if the camera gate opened at time zero and remained open for a duration equal to τ_L. In this case the gas moves during the time that the laser is on. So, the laser tags a patch of gas with a spatial width equal to $u \cdot \tau_L$. If the velocity is equal to zero (as it is in the static gas measurement performed as a reference, prior to each shot), then the width of this patch of gas is infinitesimal, and the image looks identical to the top panel.

The third panel (CCD at $t = \tau_d$) shows how the tagged gas would look if imaged by a camera delayed by τ_d and having an infinitely short gate duration. This image shows that the tagged patch of gas has translated by a distance equal to $u \cdot \tau_d$. The fourth panel (CCD from $t = \tau_d \rightarrow \tau_d + \tau_G$) shows the image that would be acquired by a camera gate that is delayed from the laser pulse by τ_d and that has a duration of τ_G. In this case the image is a convolution of the tagged patch of gas and the camera gate. The center of this trapezoidal area is displaced to the right of the left edge of the trapezoid by the distance equal to $u \cdot (\tau_L + \tau_G)/2$. This motional blurring does occur in the experimental, although in the figure it is greatly exaggerated for clarity.

In the experiment and image analysis we determine the displacement d between the static gas (an image similar to the top panel) and the image acquired during the shot (an image similar to the fourth panel). Thus, the velocity is computed according to

$$u = d/[\tau_d + (\tau_L + \tau_G)/2] \tag{3}$$

Hypersonic Boundary-Layer Flow

The laminar boundary layer that forms on a flat plate in a hypersonic flow is a relatively well-understood flowfield.[1,2] As shown in Fig. 1, a thin boundary layer grows on the flat plate. The boundary layer grows quadratically near the leading edge and linearly further downstream. The rapid growth of the boundary layer at the sharp leading edge causes a weak shock wave to form. This shock weakens as it bends downstream, as shown in the figure. One characteristic that distinguishes hypersonic boundary layers from their supersonic and subsonic counterparts is that the temperature in the boundary layer increases dramatically above the freestream temperature as viscosity converts kinetic energy to thermal energy. If the wall is thermally conducting, then the temperature in the boundary layer adjacent to the wall approaches the wall temperature.

A slight complication in the present experiment is that we used a conical nozzle. Thus, the flow continued to diverge as it passed along the flat plate. This caused a slight pressure gradient in the freestream that must be accounted for in CFD comparisons with these measurements.

Hypersonic Flow over a Blunt Fin Attached to a Flat Plate

The hypersonic flow over a blunt fin attached to a flat plate simulates the wing/body, tailfin/body, and strut/wing junctions on aerospace vehicles. We have attached a 19-mm-diam blunt fin 152 mm downstream of the leading edge of a flat plate and inserted this model into a hypersonic flow at 0-deg incidence. Similar configurations have been studied extensively with surface measurement techniques,[28,29] and recently with planar flowfield visualization methods.[30] These references and references therein can be seen for a detailed description of the flowfield. Briefly, a boundary layer forms on the flat plate. At the same time a bow shock forms on the blunt fin. The interaction between the boundary layer and the strong shock wave causes the boundary layer to separate upstream of the blunt fin. The separated flow region then induces an oblique separation shock wave on top of the separated flow region. In the separated flow region closest to the flat plate, the gas temperature is high, and reverse flow (gas travelling upstream) is expected. The goal of the present measurements was to observe this reverse flow using the new velocimetry method.

Experiment

The experiments were performed in the T2 and T3 free-piston shock tunnels at the Australian National University.[31,32] A schematic of the boundary-layer velocimetry experiment, performed in the T2 free-piston shock tunnel, is shown in Fig. 3. The nozzle had a 15-deg full-angle conical geometry with a 5.4-mm-diam throat and a 73-mm exit, resulting in an exit-to-throat area ratio of 183. The nozzle had a throat-to-exit length of 255 mm. The shock tube was filled to 100 kPa with a mixture of 98.9% N_2 and 1.1% O_2 and was at room temperature prior to tunnel operation. This gas mixture was chosen to produce an amount of NO sufficient to produce good fluorescence but that would minimize the amount of the gases (O_2, O, and NO) that are efficient quenchers. The primary shock speed was 2.4 ± 0.05 km/s, which corresponds to a flow enthalpy of 5.8 MJ/kg. The nozzle-reservoir pressure was measured to be 27.5 ± 1.5 MPa, and reservoir temperature was calculated to be 4591 K using the equilibrium shock-tube code.[33] We used the one-dimensional nonequilibrium code STUBE to estimate the nozzle-exit conditions (to be used as an inlet condition for CFD) and to estimate the freestream conditions at the measurement location.[34] At the measurement location, 65 mm downstream of the nozzle exit and 80 mm downstream of the leading edge of the flat plate, STUBE predicts a velocity of 3184 ± 80 m/s, a temperature of 362 ± 25 K, a pressure of 2.4 ± 0.2 kPa, and a Mach number of 8.52 ± 0.05. The estimated gas composition at this location was 98.3% N_2, 1.0% NO, 0.3% O_2, and 0.3% O. The Reynolds number based on the distance

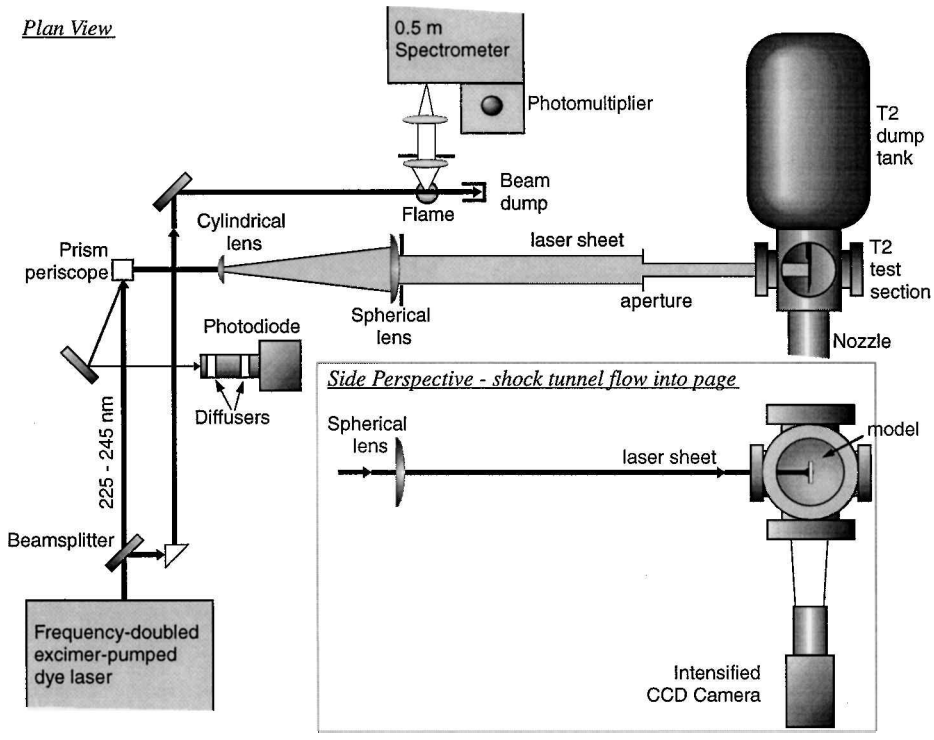

Fig. 3 Schematic of the experiment. In the present experiment the cylindrical lens was rotated by 90 deg to orient the laser sheet across the span of the flat plate. An aperture in front of the test section clipped the beam to a width of 3 mm.

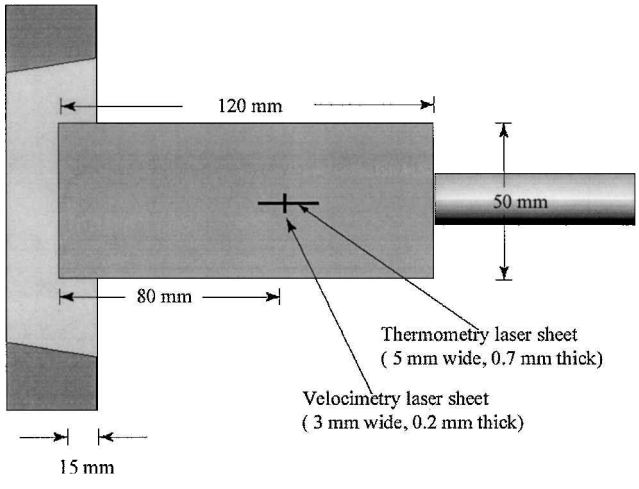

Fig. 4 Plan view of the measurement location.

from the leading edge of the flat plate to the measurement location was 27,000, whereas the critical Reynolds number for transition to turbulence in a hypersonic flow over a flat plate is 1×10^6 (Ref. 35).

During the measurement time, the T2 shock tunnel recoils 8.0 ± 0.5 mm. After recoil the tip of the flat plate was located 15 ± 0.5 mm inside the nozzle, corresponding to a distance of 240 ± 0.5 mm from the nozzle throat. As shown in Fig. 4, the flat plate was 120 mm long and had a width of 50 mm. It had a sharp leading edge and was mounted from the rear by a sting. As shown in the figure, the laser sheet in the current experiment was oriented perpendicular to the flow and parallel to the line of sight of the camera. Also shown in the figure is the orientation of the laser sheet for the thermometry experiments reported elsewhere.[4] The laser sheet was centered 80 ± 1 mm downstream of the leading edge and was measured to be 0.20 ± 0.05 mm thick.

For the measurements in the T2 shock tunnel, we frequency-doubled the output of an excimer-pumped dye laser (Lambda Physik, Scanmate II) to obtain 2-mJ, 25-ns pulses at 225 nm, coinciding with the (0,0) vibrational band of the A–X electronic transition of NO. Most of the laser light was formed into a 3-mm-wide sheet and was directed into the test section perpendicular to the flow. Approximately 1 mJ was used to form the laser sheet. A small portion of the laser beam was split off and used for wavelength calibration by performing LIF of NO generated by entrainment of nitrogen from room air into an H_2/O_2 welding torch.

Approximately a half-hour before each T2 shock tunnel run, we filled the test section with 1.7% NO in He to a pressure of about 2 kPa. The laser was tuned to the peak of the NO transition. We then obtained a LIF image of the line in the static gas to be used as a zero-velocity reference image during the analysis. Next, the test section was evacuated in preparation for a shot. Just prior to each shot we adjusted the laser to the same transition by monitoring LIF in a flame. Immediately before the shot (<5 s), the tunnel operator stopped the laser via a remote switch next to the firing valve. After the firing valve was opened, the nozzle reservoir pressure transducer detected the shock reflection at the end of the shock tube, and the laser fired 350 μs later. This delay was chosen to coincide with the period of steady flow in the shock tube.

An intensified CCD camera (Princeton Instruments, 16-bit CCD, 576×384 pixels, 30 ± 3-ns gate duration) captured the fluorescence image at right angles to the laser sheet. The image resolution was 22.4 ± 0.2 pixels per mm. A 2-mm-thick UG-5 filter was placed in front of the intensified CCD (ICCD) camera. This filter allowed the fluorescence above 230 nm to pass into the camera, but cut off most of the elastically scattered laser light and some of the flow luminosity. The filter also blocked resonant fluorescence [A–X (0,0) near 226 nm].

Some light originating from the surface of the flat-plate model is transmitted through the filter. We believe that this could be fluorescence resulting from ablation of the black paint on the model. For the last three shots of the experiment, the paint was removed, and the surface was polished, which reduced the intensity of the scatter by a factor of five. We did not want to eliminate this scattered light completely because it serves as an excellent marker for determining the location of the intersection between the laser beam and the flat plate.

For the measurements in the T2 shock tunnel, we probed the coincidental overlap of four different NO lines: $Q_2(19.5)$ and $Q_1(12.5)$ and their satellite transitions at 44,227.71 cm^{-1}. These four transitions were chosen for their appreciable ground-state populations for

all temperatures expected in the experiment as well as their strong transition probability, which results in strong fluorescence.

Considering the laser energy used, the pulse duration, the beam area, the transition line strength, and an estimate of the flow conditions, we predict that the laser irradiance is five times the saturation irradiance I_{sat} in the freestream. Higher irradiance would not increase the signal intensity significantly. For this reason we spread the laser beam out into a sheet 3 mm wide. This increases the signal intensity by a factor of ~15 compared to focusing the beam to a spot 0.2 mm in diameter because the laser energy is spread out along a line rather than further saturating the transition at a single point. The line was limited to 3 mm because this was a similar length to the camera's depth of field (~2 mm) and a wider sheet would cause the line to blur.

Other approaches were used to increase the signal-to-noise ratio in the raw images. The camera gain was increased to 9.5/10 for some of the longer delays. Also, we used the maximum lens aperture (4.5). The camera was placed as close as possible (about 30 cm) to the measurement location to collect the maximum amount of fluorescence and to provide the highest possible magnification. Furthermore, the camera was oriented slightly above the level of the flat plate so that the full area of the lens would collect fluorescence from the region closest to the plate. These measures were necessary because we estimate that $\tau_{LIF} = 140$ ns. Thus, when $\tau_d = 750$ ns, only 0.5% of the original fluorescence remains! Owing to the precautions just described, good velocity measurements were still obtained at this delay, despite the low signal levels.

Velocity measurements were also performed in a hypersonic separated flow in ANU's T3 free-piston shock tunnel. The experimental setup is described in detail elsewhere.[30] In the following we describe only the points that are distinctly different from the measurements performed in the T2 tunnel, just described. The blunt-fin model consisted of a flat plate ~200 mm wide and 245 mm long. The blunt fin was 19 mm thick, with a hemispherical leading edge, and was 158 mm long. The front of the blunt fin was mounted 152 mm downstream of the sharp leading edge of the flat plate. The model was rear mounted in the test section of the T3 free-piston shock tunnel so that the leading edge was 51 mm downstream of the nozzle exit before the 34 mm recoil and 10 mm below the centerline. The nozzle was conical with a throat diameter of 25.4 mm, an exit diameter of 305 mm, and a 15-deg full angle. The flow velocity, pressure, and temperature computed just forward of the bow shock forming on the blunt fin are 2.72 km/s, 2.83 kPa, and 325.5 K, respectively.[30] The gas composition, by mole fraction, is predicted to be 97.1% N_2, 1.2% O_2, 1.6% NO, and 0.06% O (Ref. 30). The unit Reynolds number for the experiment was 4.5×10^6 m^{-1}, which indicates that the boundary layer should be laminar before separation.

The fluorescence imaging system used for the measurements on the T3 shock tunnel is similar to that just described except that the laser source is an Nd:YAG pumped dye laser, operating at 574 nm. This light is frequency doubled and mixed with the infrared output of the Nd:YAG laser to produce up to 5-mJ pulses of 225-nm light with a duration of 9 ± 2 ns. The laser light was directed into the tunnel by several sheet-forming optics. Unfortunately, some of these optics were mounted to the shock tube and others to the laser table, which led to an unpredictable beam orientation resulting in systematic errors in the measurements. This point is discussed further in the following section. The laser sheet was 10 mm wide and approximately 0.5 mm thick and was oriented perpendicular to the flow, 28 mm upstream of the leading edge of the blunt fin and on the flow centerline. The laser frequency was tuned to the coincidental overlap between the $Q_2(30.5)$ and $R_2(24.5)$ lines of NO at 44,401.2 cm^{-1}. These transitions were chosen to provide fluorescence intensities in all flow regions of interest.

It was not deemed environmentally responsible to fill the large T3 test section and dump tank with toxic NO gas prior to each run as just described. As a result, it was not possible to obtain a zero-velocity reference image in static gas. The laser pulse was fired 1500 μs after shock reflection, which is in the middle of the steady flow time produced by the tunnel. The ICCD camera gate duration was set to 20 ns, and it was delayed 500 ns from the firing of the laser pulse. The camera gain was $\frac{10}{10}$. The magnification obtained was 19.4 ± 0.3 pixels/mm. For the measurements in the T3 shock tunnel, the camera was positioned slightly below the plane of the flat plate in order to reduce the intensity of scattered light from the flat plate. This unfortunately attenuated the fluorescence intensity in the region nearest the wall, which increased the uncertainty in the measurement.

Results and Discussion

Flat-Plate Measurements

Figure 5 shows the images obtained at four different delays in the experiment. The images are shown side by side for clarity. To enable the lower intensity values in the images to be observed, the images display the natural logarithm of the raw data. The zero-delay image was obtained in the static gas in the test section prior to a shot. The three other delays were obtained during subsequent tunnel runs. In total, 11 measurements were obtained, using seven different delays ranging from 0 to 750 ns. The laser enters each image from the top striking the flat plate located at the bottom of each image. The scattered light already mentioned from the flat plate creates a bright spot at the bottom of the images, which is clearly visible even in the three delayed images. This point provides a reference mark for zero velocity in each image.

The images clearly show that the freestream flow at the top of each image is fairly uniform. Close to the flat plate, the images show Blasius-like profiles, as expected. Note that the signal-to-noiseratio of the longer delays is significantly worse than the shorter delays. The width of the line in the zero-delay image is approximately 6.5 pixels. This is dominated by the width of the laser sheet and blurring caused by the intensifier. The width of the line in the delayed images is approximately 50% larger than the width of the zero-delay image. This increase can be attributed to the finite laser pulse duration and the finite camera gate duration, both of which act to blur the observed line (see the bottom panel of Fig. 2). The width of the line does not appear to increase with delay τ_d. This implies that thermal diffusion is not a dominant line-broadening mechanism in this experiment.

From these images we measure the displacement vs height by using the peak-fitting algorithm discussed in the Theory section. Figure 6 shows the displacement measured for shot 725, which had a delay of $\tau_d = 350$ ns. The quality of the data is very good. However, the displacement measured in the freestream is clearly sloped even though we expect a constant freestream velocity. Figure 6 also shows the displacement measured from the fluorescence image obtained in the static gas, prior to the shot. This displacement is also sloped. On each of the 11 pairs of images, these two slopes, caused by slight misalignment of the laser sheet, were approximately the same. We conclude that subtracting the two displacements accurately corrects for misalignment of the laser sheet. Figure 7 shows the corrected displacement resulting from this subtraction.

For most of the shots, the displacement could not be accurately determined within 0.3 mm of the wall because of interference from the light scattered by the model. This corresponds to the inner 15% of the boundary layer (based on the measured velocity profile). The

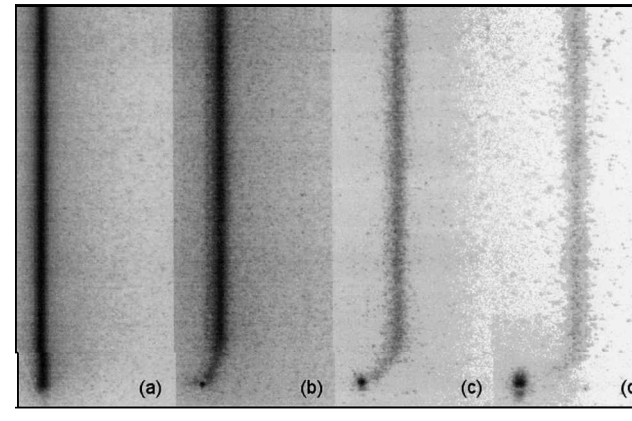

Fig. 5 Raw LIF intensities for four delays: 0, 250, 500, and 750 ns for a–d, respectively. Image a was obtained in static NO in the test section. Images b–d were obtained during the shock-tunnel flow.

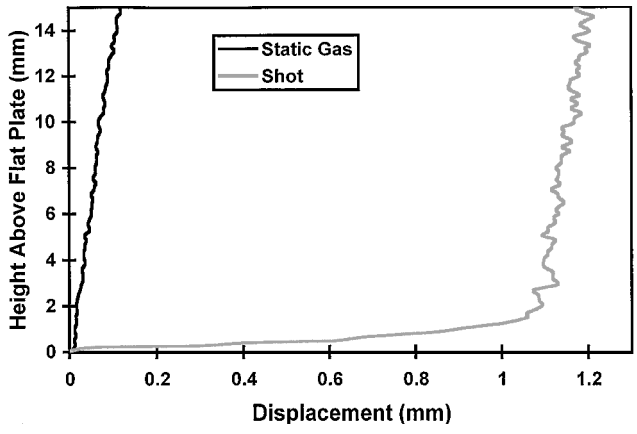

Fig. 6 Displacement measurements for shot 725 (delay of 350 ns) and for a LIF image taken prior to the shot in static NO.

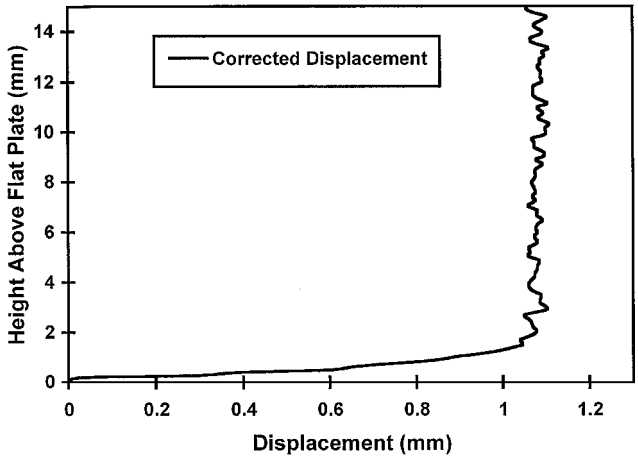

Fig. 7 Corrected displacement for shot 725.

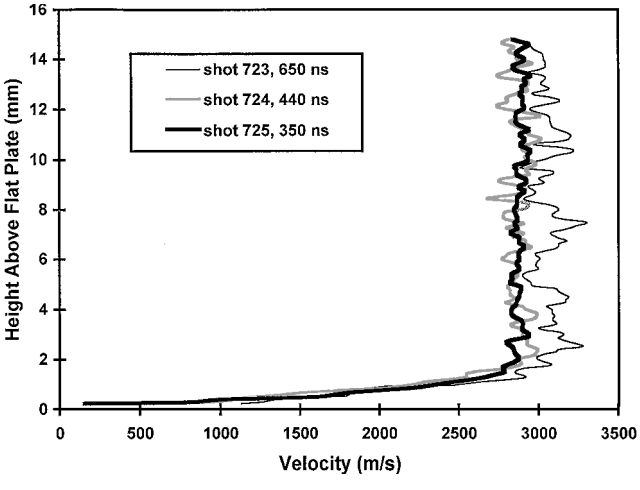

Fig. 8 Three typical single-shot velocity measurements.

image-processing algorithm jumps to this bright spot in the image, producing spurious zero-velocity results near the wall. These bad data points near the wall were examined and omitted by hand. We attempted to crop the bright spot out of the image and then to refit the data, but this gave similarly poor results. A better fitting algorithm might allow the velocity close to the wall to be determined for all images. As already mentioned, the final three measurements were much less affected by this scatter source. Consequently, these measurements of velocity were obtained slightly closer to the wall (within 0.2 mm).

Single-shot velocity profiles were determined for each shot using Eq. (3). Figure 8 shows three of the single-shot velocity measure-

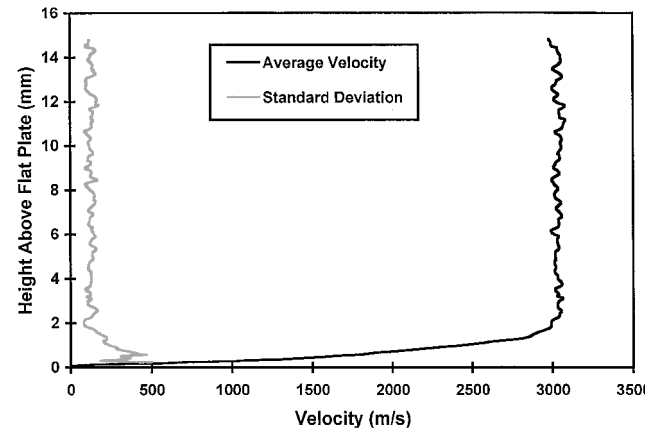

Fig. 9 Average and standard deviation of velocity profiles.

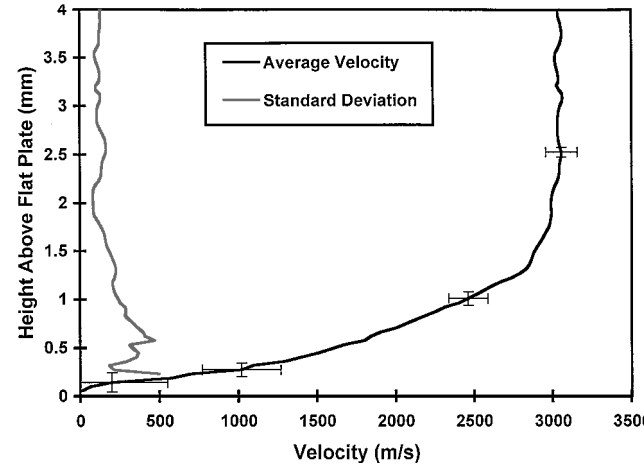

Fig. 10 Detail of measured, average velocity profile near the wall.

ments. A clear trend observed in the experiment was that longer delays τ_d gave noisier velocity profiles. However, the longer delays are not necessarily less accurate because the measurement uncertainty of the timing decreases with increasing τ_d.

We averaged the nine single-shot velocity profiles obtained from shots where $\tau_d > 0$. We also took the standard deviation of the velocities at each height along these profiles. Figure 9 shows the results. The freestream velocity is very uniform. The standard deviation of the velocity in the freestream is ~130 m/s and increases in the boundary layer. When averaged over a height of 3 to 15 mm above the flat plate, the freestream velocity is 3035 ± 100 m/s (standard error of 3.3%, with 90% confidence). This measured value of the freestream velocity agrees with the value of 3184 ± 80 m/s predicted by the STUBE flow code. Because measurements from nine tunnel shots were averaged, random error from sources such as jitter were reduced by a factor of three. Because the velocity was averaged over more than 300 pixels, random error from signal-to-noise considerations tended to zero. However, uncertainties associated with systematic errors such as camera magnification and laser/camera timing were not reduced by averaging, and these sources of error dominate the stated uncertainty. This measurement uncertainty is a substantial improvement over previous measurements obtained in the same facility using the spark tracer technique. McIntosh[36] measured the freestream velocity to be $\sim 6000 \pm 500$ m/s (uncertainty of $\pm 8\%$ with 90% confidence) at significantly different flow conditions.

Figure 10 shows a detailed view of the inner boundary layer. We determined the boundary-layer thickness from this profile. The boundary-layer thickness based on $0.95 \cdot u_\infty$ is 1.4 ± 0.1 mm.

We also used a second method to determine the freestream velocity. We plotted the average of the measured displacement from 3 to 15 mm above the flat plate for each shot against the total delay,

$\tau_d + (\tau_L + \tau_G)/2$. Then a straight line passing through the origin was fitted to the data. The resulting graph is shown in Fig. 11. Using this method results in a freestream velocity of 3087 ± 100 m/s. This agrees even better with prediction of STUBE than the value obtained by averaging the single-shot velocities.

Some of the measurement points in Fig. 11 do not fall exactly on the straight line, nor does the line fall within the error bars of the measured points, which were determined from statistical variation of the measured displacements between 3 and 15 mm above the plate. This discrepancy could be explained by shot-to-shot variation in the tunnel operating conditions. For example, the two shots with the longest delay (750 ns) fall above the line; they also have the highest recorded reservoir pressures (7% higher than the mean), resulting in the velocities slightly higher than the mean. Another explanation is that the magnification of the system could have changed slightly when the camera was refocused halfway though the experiment: the last three measurements made (at $\tau_d = 350$, 440, and 650 ns) all fall below the line.

In determining the measurement uncertainties, we considered several different sources of error. Error contributions from most of these sources are shown in Table 1. Significant random errors in the experiment include our ability to measure the shift from the image and the timing jitter in the electronics, particularly in the excimer laser. Note that the uncertainty in measuring the shift increases with delay because the signal to noise of the images decreases, whereas the relative uncertainty in the velocity caused by the timing jitter decreases with delay.

Systematic errors in the experiment included the ability to measure the magnification of the optical system and also the timing uncertainties between the laser and camera. This timing uncertainty includes the uncertainty of the laser pulse duration, uncertainty of the camera gate duration, and uncertainty of the absolute time delay between the laser pulse and the camera acquisition. We estimated these timing uncertainties to between ± 3 and ± 5 ns. The total measurement uncertainty at a single-point in an image for a single-shot measurement is then estimated at $\pm 3.5\%$, although this depends somewhat on delay. The minimum uncertainty occurs for longer delays. The uncertainties for averaged freestream velocities were quoted above at $\pm 3\%$ because averaging over many samples reduces the random error, but not the systematic errors.

Table 1 Error analysis computed for a single-shot measurement of velocity at a single point along the tagged line for $\tau_d = 250$, 500, and 750 ns

Error analysis	250 ns	500 ns	750 ns
Random errors[a]			
Measurement of shift	1.2[b]	1.8	2.2
Timing jitter (5 ns)	2.0	1.0	0.7
Total random errors[c]	2.3	2.1	2.3
Systematic errors			
Magnification	1.0	1.0	1.0
Laser/camera timing (5 ns)	2.0	1.0	0.7
Total systematic errors[c]	2.2	1.4	1.2
Overall uncertainty, %[d]	4.6	3.5	3.5
Uncertainty at 3000, m/s	137	104	105

[a]Random errors cited are based on one standard deviation.
[b]Unless otherwise indicated, the numbers are percentages.
[c]Total errors are summed quadratically for both random and systematic error sources.
[d]Overall uncertainty is computed as the linear sum of total random and systematic errors.

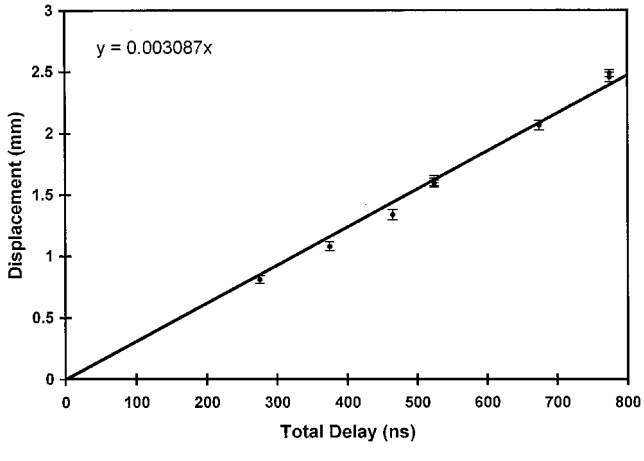

Fig. 11 Measurement of average freestream velocity by fitting a straight line through time-of-flight data.

Another possible source of error that we investigated was the radiative heating of the plate by the laser. This was tested by firing the laser directly at a coaxial thermocouple mounted in the plate and measuring the increase in temperature using the thermocouple. The laser beam occupied the same area as the active area of the thermocouple. The junction for the thermocouple was made by sanding the surface of the thermocouple until it was flush with the model surface. The very small contact area gave the thermocouple a response time of approximately 1 μs. The measured peak temperature was approximately 70 K above ambient, decaying exponentially to ambient conditions after 100 μs. The beam used in the velocimetry experiment was much narrower than this beam but had a similar irradiance. The response time of the thermocouple is still a factor of 100 slower than the pulse duration, so that the peak heating might have been greater than measured. However, the response of the flow would be on a similar timescale to the thermocouple. Calculations performed using the analytical method outlined by Haridas[37] show that for a 100 K difference in surface temperature the velocity profile varies by no more than 1.5% of the freestream velocity in the middle of the boundary layer. The variations near the wall and near the freestream are negligible.

Another possible source of error in the current experiment is that the laser beam appears to ablate a small amount of paint and metal from the flat plate during the measurement. This is observed as "laser scatter" in the images at the surface of the flat plate. The jet formed by this ablation process could alter the velocity profile. However, we believe that this effect is negligible because during the last three shots, where the model was polished and the emission at the flat plate was five times smaller, we noticed no change in the velocity profile compared to the earlier measurements. We believe that this jet causes very little perturbation to the flowfield because most of the tagged fluid quickly propagates downstream of the jet, avoiding interaction with the jet. In future experiments we could reduce this effect by decreasing the laser intensity substantially (by a factor of 5–10). This would cause the LIF signal to drop by a factor of 2 or 3, whereas the jet intensity would decrease by a factor of 5–10. One could use this approach to determine whether jetting from the model surface affects the measured velocity profile.

Reviewing the statistics of the measurements offers an interesting insight about the error sources. The freestream velocities measured within each image had an average standard deviation of 57 m/s or 1.8%. On the other hand, the standard deviation of each image's average freestream velocity was much larger: 116 m/s or 3.8%. This indicates that error sources such as timing jitter associated with subsequent measurements on different tunnel runs, or the change in camera magnification just mentioned, were more significant than random errors within a single measurement, caused by poor signal to noise in the image, for example. So, it appears that a contribution from an unknown source of tunnel-run-to-tunnel-run error has not been accounted for in Table 1. The magnitude of this random error could be as large as 3%. If this error is truly associated with the measurement technique, then the overall single-shot measurement uncertainties would be revised upward to ~5%. However, it is likely that part of this unaccounted for "error" is caused by run-to-run variations in the freestream velocity produced by shock tunnel itself, not caused by the measurement technique. Thus, Table 1 remains the best estimates of measurement uncertainties.

Blunt-Fin Measurements

To demonstrate the applicability of this method to more complicated flowfields, we measured the velocity profile in the separated flow region in front of a blunt fin attached to a flat plate in a Mach 7.4 flow. Figure 12 shows a single-shot fluorescence image obtained

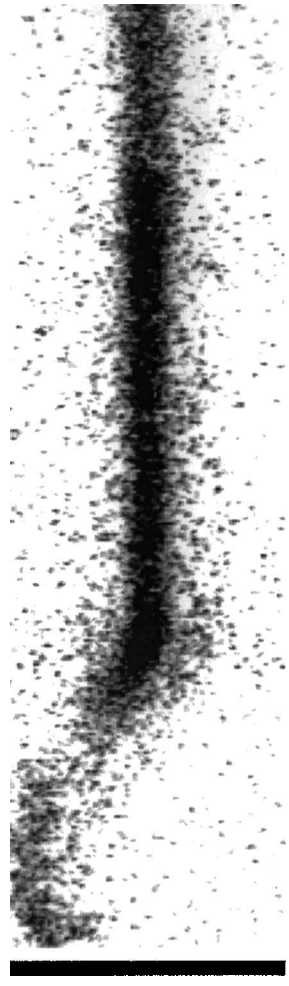

Fig. 12 Raw flow-tagging image for the separated flow forward of a blunt fin attached to a flat plate. The approximate location of the flat plate is indicated by the black line at the bottom of the image.

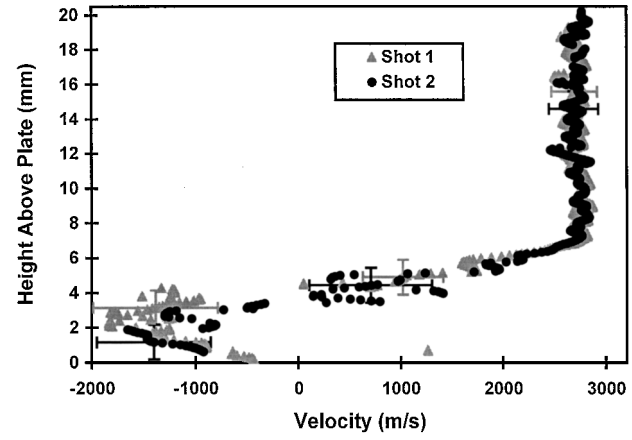

Fig. 13 Measured velocity profile 30 mm forward of a blunt fin attached to a flat plate. Reverse flow near the wall is clearly observed.

through the freestream (top) and separated flow region (middle and bottom). The laser entered the imaged region from the top and the flow direction in the freestream is from left to right. The flow nearest the wall is moving to the left. The fluorescence intensity near the flat plate is low for two reasons. First, the temperature in that part of the flow is very high (~2000 K), and the population of the probed states is small at such high temperatures. Second, the camera was oriented slightly below the plane of the flat plate to avoid viewing of the intense scattered light originating from the flat plate. As a result, much of the fluorescence near the plate was obscured. Another consequence of having the camera oriented slightly below the flat plate is that the scattered light from the flat plate is not at all visible. Thus, it cannot be used as a reference mark as described in the preceding boundary-layer measurements. Furthermore, because it was unsafe to fill the large T3 test section and dump take with nitric oxide gas to get a zero-velocity reference image prior to the shot we have no in situ calibration of the absolute velocity, nor the angle of the laser sheet for this blunt-fin data set. Instead, we have used the computed freestream velocity as a calibration point and have assumed that the laser sheet is propagating perpendicularly to the flat plate. Although this is not the ideal analysis method, the results still serve to demonstrate the fact that this velocity measurement technique can be applied to study complex flowfields.

Figure 13 shows single-shot velocity profiles measured from two successive tunnel runs. The horizontal location of the image was freely adjusted so that average freestream velocity matched the computed value of 2710 m/s. Otherwise, processing of the images was similar to the preceding boundary-layer measurements described. The resulting velocity profiles show the structure of the separated flow region, including forward flow above 7 mm, a shear layer between 3 and 7 mm, and a zero-velocity line around 4 mm above the flat plate. The maximum reverse flow velocity of about −1900 m/s occurs at ~2 mm above the flat plate, with the velocity approaching zero at the flat plate. Because no scattered light was observed at the flat plate's surface, it was difficult to identify the exact location of the flat plate. Consequently, there is a large uncertainty (±1.5 mm) in the height of the measurement, and so some caution should be exercised when interpreting these data. The uncertainty in the measured velocities is substantial (up to ±600 m/s) because of the low fluorescence intensities in the raw images. Other sources of error are small by comparison.

Several changes could be made to improve this second set of velocity measurements. First, the camera could be oriented so that the scattered light from the flat plate is observed. This would provide a laser-incidence reference point that can be used to identify zero flow velocity and to identify the location of the flat plate. This modification would also increase the fluorescence intensity near the model surface. Other measures could be taken to increase the fluorescence intensity. These include making the camera gate duration longer (say, 50 ns instead of 20 ns) and by making the camera delay shorter (say, 300 ns instead of 500 ns). These two changes would increase the signal-to-noise ratio by an order of magnitude that would reduce the uncertainty in determining the shift to a level that is more comparable with the other uncertainties in the experiment, such as timing uncertainties. It is likely that another nearby absorption transition of nitric oxide could be excited that would increase the fluorescence intensity in the hotter part of the flow. Finally, a small gas cell containing nitric oxide could have been placed in the measurement region just prior to each shot to measure the orientation of the laser sheet so that it could be corrected in image processing. Unfortunately, time limitations of the T3 shock tunnel facility prevented these changes from being implemented. Despite the large uncertainties, these measurements demonstrate that nitric-oxide fluorescence flow-tagging velocimetry is suitable for studying complex separated flowfields.

Conclusions

In conclusion, we have demonstrated flow-tagging velocimetry of NO using a single laser for the first time. We used this method to measure the velocity profile of a laminar boundary layer on a flat plate in a hypersonic flow. The average freestream velocity was measured to be 3035 ± 100 m/s, which corresponds to a measurement uncertainty of ±3.3%. To our knowledge, these are the first high-quality velocity measurements performed in a laminar hypersonic boundary layer. Furthermore, we measured the velocity profile in the separated flow region forward of a blunt fin attached to a flat plate in a hypersonic flow. The resulting measurement uncertainty for this second data set was much higher (up to ±600 m/s). Although these measurement are less accurate than would be desired for comparison with CFD, we have outlined several small changes to the experimental method that would produce more accurate results. Still, we believe that these are the first velocity measurements in such a hypersonic, separated forebody flowfield.

The major advantages of this velocity measurement technique are that it is conceptually simple and easy to interpret. It uses a single laser, whereas most flow-tagging methods use two or three

lasers. The method is especially convenient for scientists already using PLIF: velocity measurements can be performed with very few modifications to the measurement system. The major disadvantage of the method is that the molecule probed needs to have a long fluorescence lifetime. This limits the applicability of the method to specialized flow facilities, like free-piston shock tunnels, where the flow velocity is high and the gas composition can be carefully controlled. Nonetheless, this method should allow a range of velocity measurements in a variety of hypersonic flows of interest to the scientific community.

Acknowledgments

The experiments were carried out at the Australian National University as part of a research program supported by a Faculty Research Grant funded through the Australian National University. We acknowledge the helpful contribution of Paul Walsh. Also, we acknowledge Glenn Diskin, NASA Langley Research Center, for providing the image-processing routines.

References

[1]Baird, J. P., Lyons, P. R. A., and Gai, S. L., "Measurement of Density and Velocity Profiles in Non-Equilibrium Laminar Hypersonic Boundary Layers in Air," *Shock Tubes and Waves, Proceedings of the 14th International Symposium on Shock Tubes and Shock Waves*, edited by R. D. Archer and B. E. Milton, New South Wales Univ. Press, 1983, pp. 374–380.

[2]Mallinson, S. G., Gai, S. L., and Mudford, N. R., "The Boundary Layer on a Flat Plate in Hypervelocity Flow," *Aeronautical Journal*, Vol. 100, No. 994, 1996, pp. 135–141.

[3]Palma, P. C., Mallinson, S. G., O'Byrne, S. B., Danehy, P. M., and Hillier, R., "Temperature Measurements in a Hypersonic Boundary Layer Using Planar Laser-Induced Fluorescence," *AIAA Journal*, Vol. 38, No. 9, 2000, pp. 1769–1772.

[4]O'Byrne, S., Danehy, P. M., Houwing, A. F. P., Mallinson, S., and Palma, P., "Temperature and Velocity Measurements in a Hypersonic Laminar Boundary Layer," *Proceedings of the 23rd International Symposium on Shock Waves* [CD-ROM], edited by F. K. Lu, 2001, Paper 1595.

[5]Hart, R. C., Balla, R. J., and Herring, G. C., "Simultaneous Velocimetry and Thermometry of Air using Nonresonant Heterodyned Laser-Induced Thermal Acoustics," ICASE, Rept. 2000-22, Hampton, VA, May 2000.

[6]Mosedale, A. D., Elliot, G. S., Carter, C. D., and Beutner, T. J., "Planar Doppler Velocimetry in a Large-Scale Facility," *AIAA Journal*, Vol. 38, No. 6, 2000, pp. 1010–1024.

[7]Clancy, P. S., Samimy, M., and Erskine, W. R., "Planar Doppler Velocimetry: Three-Component Velocimetry in Supersonic Jets," *AIAA Journal*, Vol. 37, No. 6, 1999, pp. 700–707.

[8]Miles, R. B., and Lempert, W., "Two-Dimensional Measurement of Density, Velocity, and Temperature in Turbulent High-Speed Air Flows by UV Rayleigh Scattering," *Applied Physics B*, Vol. 51, No. 1, 1990, pp. 1–7.

[9]Seasholtz, R. G., Panda, J., and Elam, K. A., "Rayleigh Scattering Diagnostic for Dynamic Measurement of Velocity Fluctuations in High Speed Jets," AIAA Paper 2001-0847, Jan. 2001.

[10]Forkey, J. N., Lempert, W. R., and Miles, R. B., "Accuracy Limits for Planar Measurements of Flow Field Velocity, Temperature and Pressure Using Filtered Rayleigh Scattering," *Experiments in Fluids*, Vol. 24, No. 2, 1998, pp. 151–162.

[11]Danehy, P. M., Mere, P., Gaston, M. J., O'Byrne, S., Palma, P. C., and Houwing, A. F. P., "Fluorescence Measurement of the Velocity-Field Produced by the Hypersonic Separated Flow over a Cone," *AIAA Journal*, Vol. 39, No. 7, 2001, pp. 1320–1328.

[12]Hiller, B., and Hanson, R. K., "Simultaneous Planar Measurements of Velocity and Pressure Fields in Gas Flows Using Laser-Induced Fluorescence," *Applied Optics*, Vol. 27, No. 1, 1988, pp. 33–48.

[13]Paul, P. H., Lee, M. P., and Hanson, R. K., "Molecular Velocity Imaging of Supersonic Flows Using Pulsed Planar Laser-Induced Fluorescence of NO," *Optics Letters*, Vol. 14, No. 9, 1989, pp. 417–419.

[14]Allen, M., Davis, S., Kessler, W., Legner, H., McManus, K., Mulhall, P., Parker, T., and Sonnenfroh, D., "Velocity Field Imaging in Supersonic Reacting Flows near Atmospheric Pressure," *AIAA Journal*, Vol. 32, No. 8, 1994, pp. 1676–1682.

[15]Barker, P. F., Thomas, A. M., McIntyre, T. J., and Rubinsztein-Dunlop, H., "Velocimetry and Thermometry of Supersonic Flow Around a Cylindrical Body," *AIAA Journal*, Vol. 36, No. 6, 1998, pp. 1055–1060.

[16]Miles, R. B., Zhou, D., and Zhang, B., "Fundamental Turbulence Measurements by RELIEF Flow Tagging," *AIAA Journal*, Vol. 31, No. 3, 1993, p. 447.

[17]Orelmann, C., Schulz, C., and Woofrum, J., "NO-Flow Tagging by Photodissociation of NO_2. A New Approach for Measuring Small-Scale Flow Structures," *Chemical Physics Letters*, Vol. 307, No. 1/2, 1999, p. 15.

[18]Ribarov, L. A., Wehrmeyer, J. A., Batliwala, F., Pitz, R. W., and DeBarber, P. A., "Ozone Tagging Velocimetry Using Narrowband Excimer Lasers," *AIAA Journal*, Vol. 37, No. 6, 1999, pp. 708–714.

[19]Hiller, B., Booman, R. A., Hassa, C., and Hanson, R. K., "Velocity Visualization in Gas Flows Using Laser-Induced Phosphorescence of Biacetyl," *Review of Scientific Instruments*, Vol. 55, No. 12, 1984, pp. 1964–1967.

[20]Wehrmeyer, J. A., Ribarov, L. A., Oguss, D. A., and Pitz, R. W., "Flame Flow Tagging Velocimetry with 193-nm H_2O Photodissociation," *Applied Optics*, Vol. 38, No. 33, 1999, pp. 6912–6917.

[21]Dam, N., Klein-Douwel, R. J. H., Sijtsema, N. M., and ter Meulen, J. J., "Nitric Oxide Flow Tagging in Unseeded Air," *Optics Letters*, Vol. 26, No. 1, 2001, pp. 30–32.

[22]Krüger, S., and Grünefeld, G., "Stereoscopic Flow-Tagging Velocimetry," *Applied Physics B*, Vol. 69, No. 5–6, 1999, pp. 509–512.

[23]Stier, B., and Koochesfahani, M. M., "Molecular Tagging Velocimetry (MTV) Measurements in Gas Phase Flows," *Experiments in Fluids*, Vol. 26, No. 4, 1999, pp. 297–304.

[24]Lempert, W. R., Jiang, N., Sethuram, S., and Samimy, M., "Molecular Tagging Velocimetry Measurements in Supersonic Microjets," *AIAA Journal*, Vol. 40, No. 6, 2002, pp. 1065–1070.

[25]Seitzman, J. M., and Hanson, R. K., "Planar Fluorescence Imaging in Gases," *Instrumentation for Flows with Combustion*, Academic Press, Burlington, MA, 1993, pp. 405–465.

[26]Eckbreth, A. C., *Laser Diagnostics for Combustion Temperature and Species*, 2nd ed., Gordon and Breach, New York, 1996, pp. 381–465.

[27]Paul, P. H., Gray, J. A., Durant, J. L., Jr., and Thoman, J. W., Jr., "Collisional Quenching Corrections for Laser-Induced Fluorescence Measurements of NO $A^2\Sigma^+$," *AIAA Journal*, Vol. 32, No. 8, 1994, pp. 1670–1675.

[28]Korkegi, R., "Survey of Viscous Interactions Associated with High Mach Number Flight," *AIAA Journal*, Vol. 9, No. 5, 1971, pp. 771–783.

[29]Poggie, J., and Smits, A., "Wavelet Analysis of Wall-Pressure Fluctuations in a Supersonic Blunt Fin Flow," *AIAA Journal*, Vol. 35, No. 10, 1997, pp. 1597–1603.

[30]Houwing, A. F. P., Smith, D. R., Fox, J. S., Danehy, P. M., and Mudford, N. R., "Laminar Boundary Layer Separation at a Fin-Body Junction in a Hypersonic Flow," *Shock Waves Journal*, Vol. 11, No. 1, 2001, pp. 31–42.

[31]Stalker, R. J., "A Study of the Free-Piston Shock Tunnel," *AIAA Journal*, Vol. 5, No. 12, 1967, pp. 2160–2165.

[32]Stalker, R. J., "Development of a Hypervelocity Wind Tunnel," *Aeronautical Journal*, Vol. 76, No. 738, 1972, pp. 374–384.

[33]McIntosh, M. K., "Computer Program for the Numerical Calculation of Frozen Equilibrium Conditions in Shock Tunnels," Dept. of Physics, Internal Rept., Faculties, Australian National Univ., Canberra, Australia, Sept. 1968.

[34]Vardavas, I. M., "Modelling Reactive Gas Flows Within Shock Tunnels," *Australian Journal of Physics*, Vol. 37, No. 2, 1984, pp. 157–177.

[35]He, Y., and Morgan, R. G., "Transition of Compressible High Enthalpy Boundary Layer Flow over a Flat Plate," *Aeronautical Journal*, Vol. 98, No. 2, 1994, pp. 25–33.

[36]McIntosh, M. K., "Freestream Velocity Measurements in a High Enthalpy Shock Tunnel," *Physics of Fluids*, Vol. 14, No. 6, 1971, pp. 1100–1102.

[37]Haridas, A. K., "Morphology of Compressible Laminar Boundary Layers," M.S. Thesis, Graduate College, Univ. of Oklahoma, Norman, OK, 1995.

R. P. Lucht
Associate Editor